JACS
JOURNAL OF THE AMERICAN CHEMICAL SOCIETY
Article
pubs.acs.org/JACS

Exceptional Single-Molecule Transport Properties of Ladder-Type Heteroacene Molecular Wires

Zhengxu Cai,[†] Wai-Yip Lo,[†] Tianyue Zheng, Lianwei Li, Na Zhang, Yubing Hu, and Luping Yu*

Department of Chemistry and the James Franck Institute, The University of Chicago, 929 East 57th Street, Chicago, Illinois 60637, United States

Supporting Information

ABSTRACT: A series of ladder-type fused heteroacenes consisting of thiophenes and benzothiophenes were synthesized and functionalized with thiol groups for single-molecule electrical measurements via a scanning tunneling microscopy break-junction method. It was found that this molecular wire system possesses exceptional charge transport properties with weak length dependence. The tunneling decay constant β was estimated to be 0.088 and 0.047 Å^{-1} under 0.1 and 0.5 bias, respectively, which is one of the lowest β values among other non-metal-containing molecular wires, indicating that a planar ladder structure favors charge transport. Transition voltage spectroscopy showed that the energy barrier decreases as the length of the molecule increases. The general trend of the energy offsets derived from the transition voltage via the Newns−Anderson model agrees well with that of the Fermi/HOMO energy level difference. Nonequilibrium Green's function/density functional theory was used to further investigate the transport process in these molecular wires.

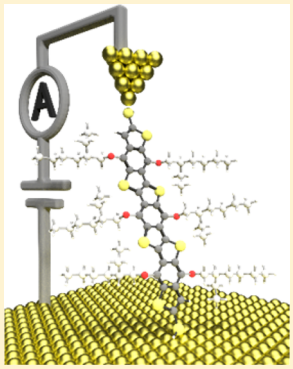

INTRODUCTION

Fundamental understanding of controlling charge transport through single molecules is the central theme of molecular electronics.[1−4] In particular, how to design molecules that allow efficient charge transport over extended distance is one of the important goals in the realization of molecular electronics. The distance dependence of the single-molecule conductance is characterized by the tunneling decay constant, β. It was observed that electron conductance decreases exponentially as a function of the molecular length, $\sigma_M \propto e^{-\beta L}$, where σ_M is the single-molecule conductance and L is molecular length.[5,6] The lower the β value, the better the molecule is able to mediate long-range charge transport. It was shown that π-conjugated molecules typically have lower β value than aliphatic σ-bond molecules. The delocalization of orbitals and the small energy gap between the highest occupied molecular orbitals (HOMO) and the lowest unoccupied molecular orbitals (LUMO) allow π-conjugated molecules to function as highly conductive wires. The Fermi energy level of the metal electrodes typically locates within the band gap of these molecules with small offset relative to either the HOMO or the LUMO, resulting in efficient charge injection and transport.

Numerous molecules were investigated, and the length dependence of their conductance can usually fit with the equation above. For example, oligothiophenes are among the most studied materials in molecular electronics due to their highly conjugated π-orbitals and efficient charge transport.[7] Other structural factors, such as effects of side chains and terminal groups on charge transport in oligothiophenes have been studied.[8−12] The conductance indeed showed exponential decay as a function of length. Interestingly, it was shown that simple tetrathiophene exhibits higher conductance than the terthiophene.[13,14] The observation was attributed to the difference in the HOMO alignment relative to the Fermi level of gold electrodes by Tao et al.[13] Campos et al. argue for the contribution due to the change in molecular conformation during the scanning tunneling microscopy (STM) break-junction experiment.[14] Most recently, Xiang et al. observed that iodide-terminated oligothiophene molecules do not follow the exponential length dependence due to transition in binding geometry to the electrodes with change in molecular length.[15]

Most recently, we have synthesized a series of new fused heteroacene molecules.[16,17] These molecules can be easily functionalized with thiol groups, offering us the opportunity to investigate the length dependence of conductance through these ladder-type molecules. The fused structure of these molecular wires locks the π-system in a single planar conformation and eliminates the uncertainty caused by the conformational change typical in oligothiophene and other linear π-conjugated systems during transport through the junction.[14] In this work, five molecules were synthesized and the number of rings in these fused heteroacenes is 3, 5, 7, 9, and 11 with names and structures as shown in Figure 1. Thiol groups are installed on the two ends of these molecules and protected with acetyl groups, which can be easily deprotected with ammonium hydroxide to form the free thiols for further immobilization onto the gold surface. All molecules except HA7 are symmetrical in the conducting backbone with ethylhexyl branched side chains to solubilize the molecules.

Received: June 10, 2016
Published: August 4, 2016

DOI: 10.1021/jacs.6b05983
J. Am. Chem. Soc. 2016, 138, 10630−10635

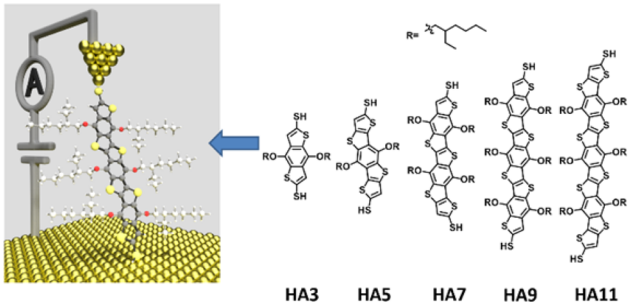

Figure 1. Experimental setup. Chemical structure of the heteroacene molecular wires and a representation of metal−molecule−metal junction in the STM break-junction technique.

RESULTS AND DISCUSSION

Synthesis and characterizations of these heteroacene (HA) molecular wires can be found in the Supporting Information. Thiol−gold binding chemistry was utilized to prepare a self-assembled monolayer (SAM) of the thiol molecules in order to measure their single-molecule conductance.[18] Successful immobilization of these molecules onto gold surfaces was confirmed by the X-ray photoelectron spectroscopy (XPS) characterizations and cyclic voltammetry (CV) measurements (Supporting Information Figures S2 and S3).

The break-junction technique with a modified STM system was utilized to measure the single-molecule transport properties.[19−21] The experiments were conducted at a bias voltage of 0.1 V in degassed mesitylene. The conductance−distance traces of the molecules with different lengths were recorded by a program written in LabVIEW. The typical conductance−distance decay curves for the heteroacene molecular junctions with different lengths are shown in Figure 2a. The conductance plateaus located ca. 10^{-4} G_0 are the characteristic signatures of single-molecule junctions, where G_0 is the conductance quantum $2e^2/h$ (e is the charge of the electron, and h is the Planck constant). Measurements were performed repeatedly to provide a statistical analysis of the single-molecule junction. A conductance histogram can be generated by compiling the effective conductance−distance curves, as shown in Figure 2b. A clear single peak can be observed for each of the molecules measured, which was fitted by a Gaussian function to determine the corresponding conductance values. The values of the single-molecule conductance of HA3, HA5, HA7, HA9, and HA11 under a bias voltage of 0.1 V were determined to be 8.08×10^{-4} G_0, 5.14×10^{-4} G_0, 4.05×10^{-4} G_0, 2.81×10^{-4} G_0, and 1.84×10^{-4} G_0, respectively. A plot of $\ln(G_0)$ versus length can be constructed with these conductance values and the corresponding lengths of the molecular wires, as shown in Figure 2c. The slope of the linear fitting represents the length-dependent decay constant β at that particular voltage. At low bias, a β value of 0.088 ± 0.007 Å^{-1} was obtained for this series of heteroacene molecular wires. These are one of the lowest β values, significantly lower than other π-conjugated molecules such as oligophenylenes (0.43 Å^{-1}), oligothiophenes (0.16 and 0.4 Å^{-1}), and cyclopentadifluorenes (0.21 Å^{-1}).[8,22] The results indicate that the ladder structure with a locked π-system together with a thiophene unit can support efficient charge transport over a long distance.

To further understand the charge transport behavior of these heteroacene molecular wires, the current−voltage (I−V) characteristics of these molecular junctions were investigated. The Au tip of the STM probe head was briefly held in the

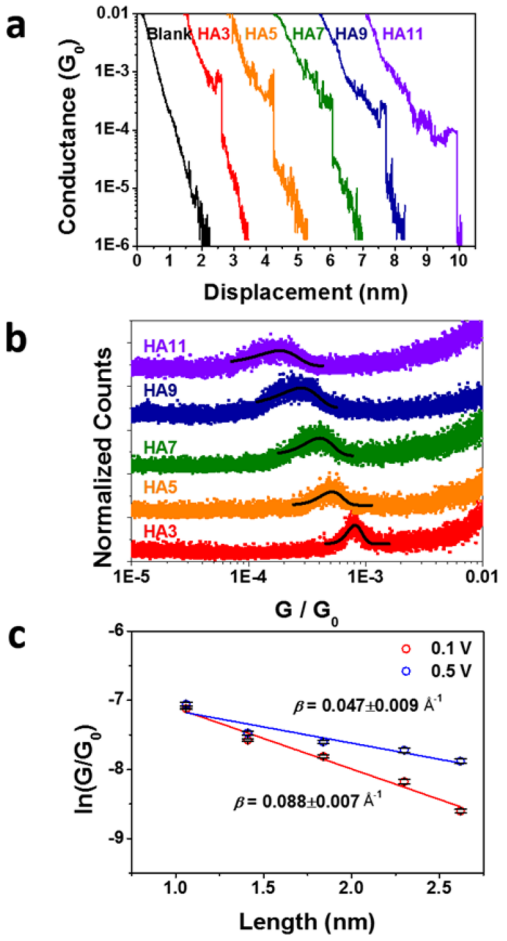

Figure 2. Molecular conductance of heteroacene wires. (a) Typical molecular conductance−distance traces of the five heteroacene molecular junctions. (b) Conductance histograms with Gaussian fitting. (c) Plot of $\ln(G_0)$ vs length of the junctions at 0.1 and 0.5 bias. Solid line is the linear fit, with slopes corresponding to the β value.

position, corresponding to the plateau in the conductance−distance curve and indicating a single molecular junction, while a voltage sweeps between +1.5 V and −1.5 V. The current−voltage characteristics of molecular junctions were repeatedly measured for a statistical evaluation and are shown in Figure 3. Details of the measurement can be found in the Experimental Section. Nonlinearity between the current and the bias voltage in the I−V curves is clearly observed, consistent with the corresponding bowl-shaped conductance−voltage (G−V) histograms (Figure 3b). As the molecule length of the heteroacene increases, the current increases more rapidly with voltage. This is more clearly observed in the G−V histogram through the increased curvature of the G−V bands from HA3 to HA11. In addition, the most probable conductance of the heteroacene wires at higher voltage can be obtained from the G−V histograms, and the results are plotted alongside the low bias conductance in Figure 2c, from which the decay constant of the heteroacene molecular wire system at 0.5 bias voltage was determined to be 0.047 ± 0.009 Å^{-1}. This value is smaller than that obtained at 100 mV bias voltage, showing a decrease in length dependence of these heteroacene molecules at higher bias.

The single-molecule transition voltage spectroscopy (TVS) can be obtained by plotting $\ln(I/V^2)$ as a function of $1/V$, also known as the Fowler−Nordheim plot.[21,23−25] The minimum of

DOI: 10.1021/jacs.6b05983
J. Am. Chem. Soc. 2016, 138, 10630−10635

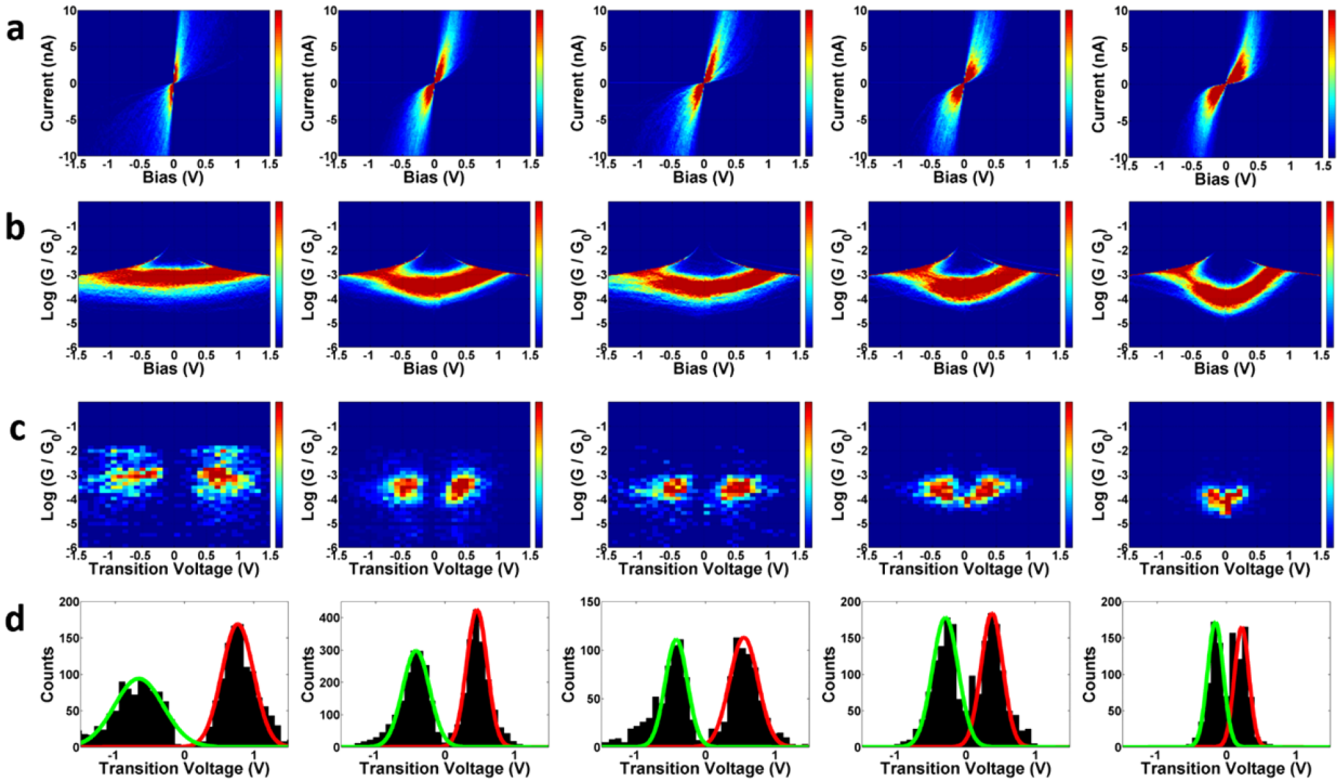

Figure 3. Current−voltage measurements. (a) Current−voltage histogram, (b) conductance−voltage histogram, (c) transition voltage histogram, and (d) 1D transition voltage histogram of HA3, HA5, HA7, HA9, and HA11 (from left to right).

the plot corresponds to transition voltage V_t. Plot of these voltages with their corresponding conductance results in the 2D transition voltage spectra shown in Figure 3c, which can be converted to 1D histograms, as shown in Figure 3d, for extracting V_t data. The transition voltage histograms of the series show a decrease in V_t as the length of the molecular wire increases, from 0.73 V for HA3 to 0.21 V for HA11. The peak locations of the transition voltages are fairly symmetrical in values between the forward and the reverse bias sweep. These values are quite low compared to those of other π-conjugated molecules.[21,26,27]

To understand the implication of these results, the Newns−Anderson model was employed to analyze the transport data, assuming that the transport is dominated by a single orbital.[28−30] For hole-transporting material, the assumption implies that the LUMO and the HOMO−1 are sufficiently far away from the Fermi level of the electrodes. The charge transport can be described as an off-resonant coherent tunneling process with a simple energy offset $\varepsilon_h = E_F - E_{HOMO}$, where E_F is the Fermi level of the electrode. When a bias V is applied to the junction, the energy offset between the Fermi level of electrodes and the energy level of the transport orbital can be approximated as $\varepsilon_h(V) = \varepsilon_h - \gamma eV$, where voltage division factor γ was derived to account for the asymmetric $I-V$ characteristics and, consequently, the transition voltages due to the polarity of the bias. Thus, the experimentally measured transition voltages $V_{t\pm}$ for both bias polarities can be used to calculate the corrected energy offset ε_h and γ using the equations developed by Bâldea.[31,32] For junctions with symmetrical $I-V$ characteristics (i.e., $\gamma = 0$), the expression for the transition voltage can be simplified as $eV_t = 2\varepsilon_h/\sqrt{3}$. The calculated values of the energy offset ε_h for the HA molecular wires are plotted against the molecular length in Figure 4a as the red data points. The absolute values of all voltage division factors γ are <0.01, with the exception of HA7 (0.018), due to the asymmetric feature of the molecular wire. Also shown in Figure 4a is a comparison of the energy offsets calculated using the transition voltages obtained from the STM break-junction experiments (red) with the energy difference between the Fermi level of gold (−5.0 eV) and the HOMO energy levels of the protected molecular wires measured by cyclic voltammetry (black). The energy offsets derived from the transition voltages follow the same trend as those obtained from CV measurements: energy offset decreases as the length of the molecule increases. As the conjugation of the molecule extends, the energy gap becomes narrower. This brings the HOMO of the molecule closer to the Fermi level of the metal electrode, resulting in smaller energy offset. In addition, the increased number of electron-donating alkoxy side chains in the longer molecules makes the molecule more electron-rich, resulting in the increase in the HOMO energy level. The energy diagram of the molecules obtained by optical and electrical characterizations shown in Figure 5 clearly illustrated this point.

To further study the correlation between molecule length and transition voltage, the dependence of the parameter $\chi = |E_F - E_{HOMO}|/V_t$ on molecular length was investigated (Figure 4b)[33,34] This parameter can reveal the relationship between the transition voltage and the energy offset of the transport orbital. For shorter molecules (i.e., HA3, HA5, HA7), the value of χ exhibits narrow variation. This is a reflection of the strong screening effect in conjugated molecules.[35,36] The π-electrons are delocalized throughout the conjugated molecule and can screen out the voltage, resulting in a voltage drop near the contacts of the junction. The χ value is relatively well-defined in this region. However, TVS becomes increasingly inaccurate for

DOI: 10.1021/jacs.6b05983
J. Am. Chem. Soc. 2016, 138, 10630−10635

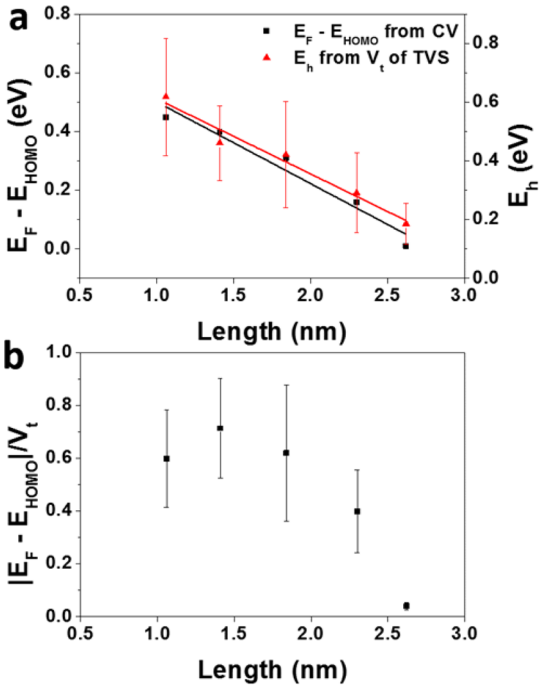

Figure 4. Energy offset comparisons. (a) Energy offsets obtained from the difference of the Fermi level of gold and the HOMO from CV measurements (black squares, left axis) are compared with those obtained from the transition voltage in the break-junction experiment using the Newns–Anderson model (red triangles, right axis). (b) Plot of $\chi = |E_F - E_{HOMO}|/V_t$ versus molecule length.

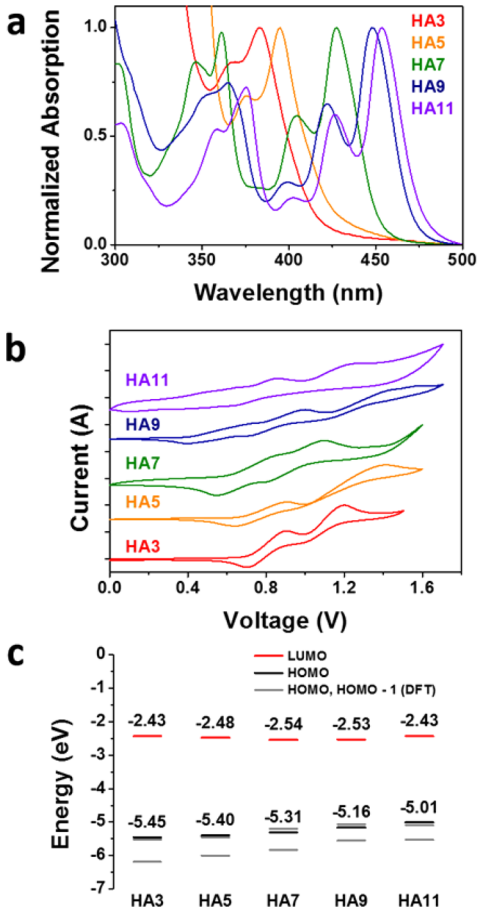

Figure 5. Wire molecule characterizations. (a) UV–vis spectra and (b) cyclic voltammograms of the five fused ring heteroacene molecular wires. (c) Energy diagram of the molecular wires showing the HOMO (black) and the LUMO (red) derived from UV–vis and CV measurements, along with the HOMO and the HOMO−1 levels obtained by DFT calculations (gray).

determining the HOMO energy offset as the transport orbital locates closer to the Fermi energy of the electrode, as shown by the small χ value for HA11 in Figure 4b.

Transport calculations based on the nonequilibrium Green's function/density functional theory (NEGF-DFT) method offer further insight into the states involved in the transport in the HA molecular wires. Geometries of each junction are optimized with DFT calculations before the transport calculation is performed. Figure 6b shows the calculated low bias transmission spectra of HA3–HA11. The main peak at ∼−1.5 eV corresponds to transport through the HOMO, while the peak at >0.5 eV corresponds to transport through the LUMO. The shorter molecular wires (e.g., HA3) having a larger HOMO–LUMO gap exhibit higher transmission but over a narrower range, while longer molecular wires have lower transmission over a wider range. As the length of the molecular wire increases, additional high transmission states emerge close to the HOMO of the junction. Their contribution to hole transport is not included in the single-level analysis in the Newns–Anderson model. Figure 6c–f shows that these additional states correspond to the lower energy orbital of the molecules. The geometries of the transmission eigenstates of the junctions match up with those of the HOMO−1 and the HOMO of the molecule itself. The HOMO−1 eigenstate also shows larger electron density on the tip Au atoms in both HA9 and HA11 junctions. Bias applied on the junction brings the frontier orbitals closer to the electrode Fermi level, including the HOMO−1 orbital. This becomes significant for the longer molecules as their HOMO/HOMO−1 gaps are smaller due to extended conjugation (Figure 5c), which may possibly allow more efficient transport through the HOMO−1 level at higher bias. The I–V curves shown in Figure S4d,e indeed show fine features in the dI/dV spectra. However, caution must be exercised in assigning these features. More experiments, especially those at low temperature, are needed to firmly designate these features to contributions from HOMO−1 transport. Further simulation of the I–V curve of the HA11 junction indicates that the calculation is consistent with the experimental data, as shown in Figure 6g. The experimental I–V curve of HA11 was compiled from the average of 25 individual curves from the STM experiment. Agreement between the experimental and the theoretical data demonstrates that the calculated transmission spectra properly depict the transmission states involved in the transport process of these molecular junctions.

CONCLUSION

In summary, we have designed and synthesized a new series of ladder-type fused heteroacene molecular wires with varying lengths. The fused ring structure prevents possible conformation change as discussed by other studies, allowing a more defined structure in the molecular core for charge transport. The length-dependent decay constant β was found to be 0.088 ± 0.007 Å^{-1} under low bias and 0.047 ± 0.009 Å^{-1} under 0.5 V. These β values are significantly lower compared to those with oligothiophene, resulting in reduced loss in conductance over a long distance. TVS analysis indicates that energy offsets

DOI: 10.1021/jacs.6b05983
J. Am. Chem. Soc. 2016, 138, 10630–10635

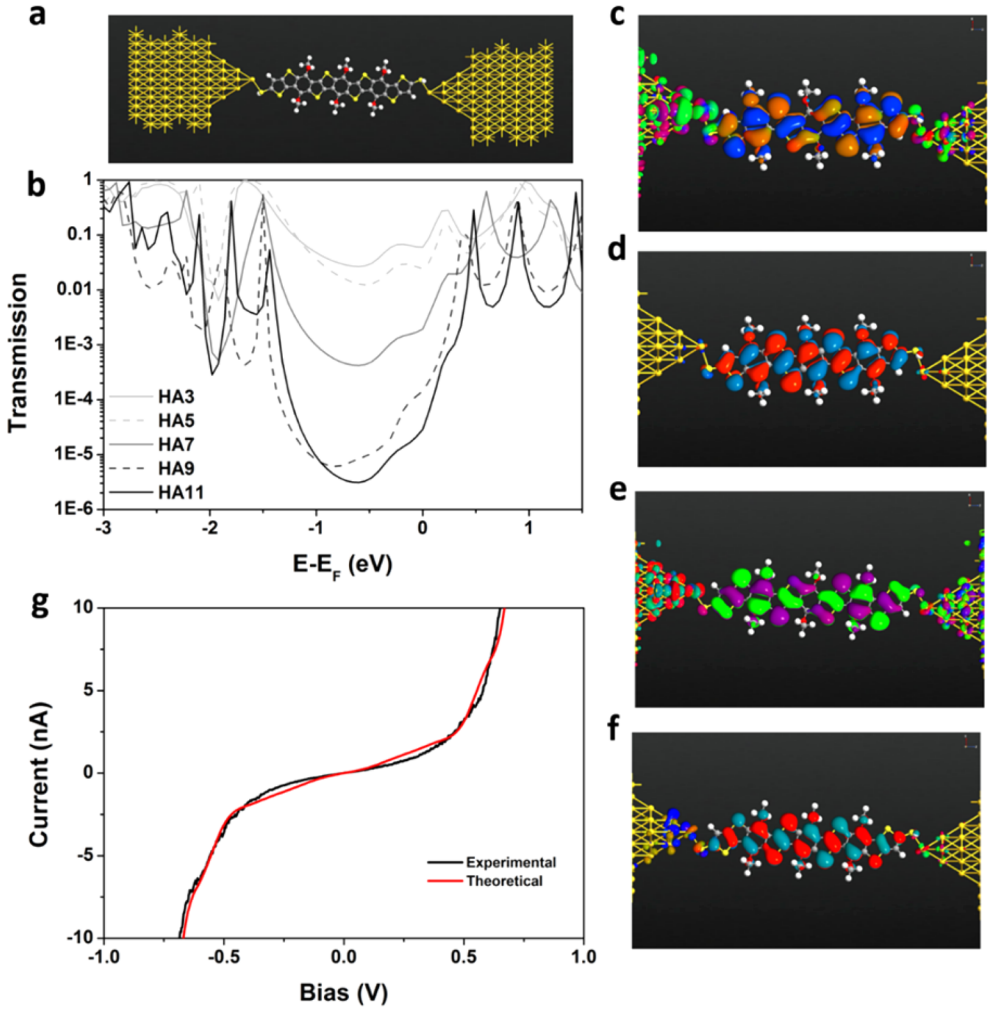

Figure 6. Transmission spectra and eigenstate calculations. (a) Example junction geometry of HA11 after optimization used in the calculations of the transmission spectra. (b) Low bias transmission spectra of the five molecular junctions. Geometries of the transmission eigenstates for HA9 that correspond to (c) HOMO−1 and (d) HOMO and for HA11 that correspond to (e) HOMO−1 and (f) HOMO. (g) Comparison between experimental and theoretical *I*−*V* curves. The experimental *I*−*V* curve is an average of 25 individual curves of the HA11 junction. The theoretical calculation agrees well with the experimental data.

decrease as the molecule lengths increase due to extended conjugation.

EXPERIMENTAL SECTION

Preparation of Self-Assembled Monolayers. Prior to each experiment, the substrate was briefly annealed in a propane flame. The SAMs of the five molecules were prepared in a single step using ammonium hydroxide (28% NH_3 in H_2O) as the deprotecting agent under a N_2 protected environment in a tetrahydrofuran (THF) solution containing ca. 5×10^{-5} M of the target molecule. A gold substrate was immersed in the solution for 12 h. The substrate was then washed successively with THF and ethanol, dried under a stream of N_2, and immediately used for the experiment.

Break-Junction Experiment for Single-Molecule Junctions. The STM break-junction experiments were conducted with a published modified STM break-junction setup. Fresh gold tips were prepared by mechanically cutting a 0.25 mm diameter gold wire (99.998% Alfa Aesar). The experiments were carried out in degassed mesitylene (≥99.9% Sigma-Aldrich). The STM Teflon solvent holder was sonicated in acetone and dried with N_2 before use. During measurement, the solvent holder was secured above the gold−SAM surface and filled with a couple drops of mesitylene. A typical break-junction experiment consisted of ca. 2000 current−distance traces. Of these traces, ∼50% displayed the conductance plateaus signifying the formation of a molecular junction and were used for the construction of the histograms. The break-junction experiments were conducted at a bias of 100 mV.

***I*−*V* Recording for Single-Molecule Junctions.** The *I*−*V* recording experiments were carried out at 100 mV of bias voltage in mesitylene. The entire process consists of iterations of three steps (tapping, conductance step detection, and *I*−*V* recording), which is in contrast to the single-step tapping procedure used in the STM break-junction measurements. In the tapping step, the tip is moved toward the substrate until the current reaches a preset threshold and then is retracted until it reaches a lower preset current. In the present method, the conductance step detection is applied during each retraction cycle to identify conductance steps. The measured conductance range was selected according to the previously measured conductance histogram of each molecule. Once a conductance step is detected, the *I*−*V* recording step is activated, which involves the following substeps: (1) the tip is immediately held in position; (2) the current−voltage curve is recorded from +1.8 V to −1.8 V quickly (10 Hz); (3) upon completion of the *I*−*V* curve, the tip is pulled away from the substrate until the current drops to a preset value, and the measurement starts over again.

Theoretical Calculations. Electron transport calculations for HA3−HA11 were performed with the nonequilibrium Green's function/density functional theory method via the Atomistix Toolkit package. Self-consistent calculations were performed using a double-ζ

DOI: 10.1021/jacs.6b05983
J. Am. Chem. Soc. 2016, 138, 10630−10635

polarized basis set, except for the gold atoms in the electrodes for which a single-ζ polarized basis set was used. Exchange correlation was treated using the local spin density approximation, and all atoms were relaxed such that the force per atom was less than 0.05 eV/Å. The k-point samplings of 3 × 3 × 50 were employed for all junction calculations, with 50 being in the direction along the transport.

■ ASSOCIATED CONTENT

Supporting Information

The Supporting Information is available free of charge on the ACS Publications website at DOI: 10.1021/jacs.6b05983.

Synthesis of the molecular wires; XPS and CV surface characterizations; average $I-V$ curves and dI/dV spectra; DFT calculations (PDF)

■ AUTHOR INFORMATION

Corresponding Author

*lupingyu@uchicago.edu

Author Contributions

†Z.C. and W.-Y.L. contributed equally.

Notes

The authors declare no competing financial interest.

■ ACKNOWLEDGMENTS

This work was mainly supported by NSF Grant No. CHE-1503852 and partially by NSF Grant No. DMR-1263006. This work also benefited from NSF MRSEC at the University of Chicago, and partially supported by the Air Force Office of Scientific Research.

■ REFERENCES

(1) Aviram, A.; Ratner, M. A. *Chem. Phys. Lett.* **1974**, *29*, 277−283.
(2) Nitzan, A. *Annu. Rev. Phys. Chem.* **2001**, *52*, 681−750.
(3) Ng, M.-K.; Lee, D.-C.; Yu, L. *J. Am. Chem. Soc.* **2002**, *124*, 11862−11863.
(4) Lo, W.-Y.; Bi, W.; Li, L.; Jung, I. H.; Yu, L. *Nano Lett.* **2015**, *15*, 958−962.
(5) Simmons, J. G. *J. Appl. Phys.* **1963**, *34*, 1793−1803.
(6) Metzger, R. M. *Chem. Rev.* **2015**, *115*, 5056−5115.
(7) Zhang, L.; Colella, N. S.; Cherniawski, B. P.; Mannsfeld, S. C. B.; Briseno, A. L. *ACS Appl. Mater. Interfaces* **2014**, *6*, 5327−5343.
(8) Yamada, R.; Kumazawa, H.; Noutoshi, T.; Tanaka, S.; Tada, H. *Nano Lett.* **2008**, *8*, 1237−1240.
(9) Leary, E.; Hobenreich, H.; Higgins, S. J.; van Zalinge, H.; Haiss, W.; Nichols, R. J.; Finch, C. M.; Grace, I.; Lambert, C. J.; McGrath, R.; Smerdon, J. *Phys. Rev. Lett.* **2009**, *102*, 086801.
(10) Lörtscher, E.; Gotsmann, B.; Lee, Y.; Yu, L.; Rettner, C.; Riel, H. *ACS Nano* **2012**, *6*, 4931−4939.
(11) Ie, Y.; Endou, M.; Lee, S. K.; Yamada, R.; Tada, H.; Aso, Y. *Angew. Chem., Int. Ed.* **2011**, *50*, 11980−11984.
(12) Zhitenev, N. B.; Meng, H.; Bao, Z. *Phys. Rev. Lett.* **2002**, *88*, 226801.
(13) Xu, B. Q.; Li, X. L.; Xiao, X. Y.; Sakaguchi, H.; Tao, N. J. *Nano Lett.* **2005**, *5*, 1491−1495.
(14) Capozzi, B.; Dell, E. J.; Berkelbach, T. C.; Reichman, D. R.; Venkataraman, L.; Campos, L. M. *J. Am. Chem. Soc.* **2014**, *136*, 10486−10492.
(15) Xiang, L.; Hines, T.; Palma, J. L.; Lu, X.; Mujica, V.; Ratner, M. A.; Zhou, G.; Tao, N. *J. Am. Chem. Soc.* **2016**, *138*, 679−687.
(16) Zheng, T.; Lu, L.; Jackson, N. E.; Lou, S. J.; Chen, L. X.; Yu, L. *Macromolecules* **2014**, *47*, 6252−6259.
(17) Zheng, T.; Cai, Z.; Ho-Wu, R.; Yau, S. H.; Shaparov, V.; Goodson, T., III; Yu, L. *J. Am. Chem. Soc.* **2016**, *138*, 868−875.
(18) Love, J. C.; Estroff, L. A.; Kriebel, J. K.; Nuzzo, R. G.; Whitesides, G. M. *Chem. Rev.* **2005**, *105*, 1103−1169.
(19) Díez-Pérez, I.; Hihath, J.; Lee, Y.; Yu, L.; Adamska, L.; Kozhushner, M. A.; Oleynik, I. I.; Tao, N. *Nat. Chem.* **2009**, *1*, 635−641.
(20) Xu, B.; Tao, N. J. *Science* **2003**, *301*, 1221−1223.
(21) Guo, S. Y.; Hihath, J.; Diez-Perez, I.; Tao, N. J. *J. Am. Chem. Soc.* **2011**, *133*, 19189−19197.
(22) Su, T. A.; Neupane, M.; Steigerwald, M. L.; Venkataraman, L.; Nuckolls, C. *Nat. Rev. Mats.* **2016**, *1*, 16002.
(23) Beebe, J. M.; Kim, B.; Gadzuk, J. W.; Daniel Frisbie, C.; Kushmerick, J. G. *Phys. Rev. Lett.* **2006**, *97*, 026801.
(24) Huisman, E. H.; Guédon, C. M.; van Wees, B. J.; van der Molen, S. J. *Nano Lett.* **2009**, *9*, 3909−3913.
(25) Stern, T. E.; Gossling, B. S.; Fowler, R. H. *Proc. R. Soc. London, Ser. A* **1929**, *124*, 699−723.
(26) Guo, S.; Zhou, G.; Tao, N. *Nano Lett.* **2013**, *13*, 4326−4332.
(27) Xie, Z.; Bâldea, I.; Smith, C. E.; Wu, Y.; Frisbie, C. D. *ACS Nano* **2015**, *9*, 8022−8036.
(28) Muscat, J. P.; Newns, D. M. *Prog. Surf. Sci.* **1978**, *9*, 1−43.
(29) Schmickler, W. A. *J. Electroanal. Chem. Interfacial Electrochem.* **1986**, *204*, 31−43.
(30) Bâldea, I. *Europhys. Lett.* **2012**, *99*, 47002.
(31) Bâldea, I. *Chem. Phys.* **2012**, *400*, 65−71.
(32) Bâldea, I. *Phys. Rev. B: Condens. Matter Mater. Phys.* **2012**, *85*, 035442.
(33) Chen, J.; Markussen, T.; Thygesen, K. S. *Phys. Rev. B: Condens. Matter Mater. Phys.* **2010**, *82*, 121412.
(34) Mirjani, F.; Thijssen, J. M.; van der Molen, S. J. *Phys. Rev. B: Condens. Matter Mater. Phys.* **2011**, *84*, 115402.
(35) Liang, G. C.; Ghosh, A. W.; Paulsson, M.; Datta, S. *Phys. Rev. B: Condens. Matter Mater. Phys.* **2004**, *69*, 115302.
(36) Liu, R.; Ke, S. H.; Yang, W.; Baranger, H. U. *J. Chem. Phys.* **2006**, *124*, 024718.

DOI: 10.1021/jacs.6b05983
J. Am. Chem. Soc. 2016, 138, 10630−10635